IV. SOLID STATE PHYSICS

Prof. W. P. Allis
Prof. S. C. Brown
Prof. C. W. Garland
Prof. G. G. Harvey
Dr. E. R. Pike
G. Ascarelli
T. Higier
L. L. Isaacs
R. G. Newburgh
J. Silverman
R. Weber

A. FOCUSING PROPERTIES OF A $\frac{3\pi}{2}$ ELECTRON SPECTROMETER FOR STUDIES OF PHOTOELECTRIC EMISSION EXCITED BY SOFT X-RAYS

1. Introduction

The energy distributions of electrons emitted from irradiated surfaces have been studied by many workers. Two main methods have been used, the "stopping-potential" method, and the magnetic-analysis method. In the first method the specimen may be in the form of a very small sphere placed at the center of a much larger spherical collector electrode, or, alternatively, may constitute one plate of a parallel-plate condenser arrangement, the second plate being the collector. The currents to the collector electrodes, plotted as a function of retarding voltage, give distribution functions from which energy distributions may be obtained by one or more graphical or electronic differentiating procedures. In the second method it has been common practice to use a 180°, uniform-field, magnetic analyzer with the specimen in the form of a narrow strip. The collector currents obtained with this method are much less than those that are available with the stopping-potential method, and the required apparatus is more complicated, but the energy distribution can now be observed directly.

Two advances have been made in electron spectroscopy since most of the earlier work was done; for example, the introduction and widespread use of the "quantum" detector, and the development of fully focusing magnetic-analyzer fields. Recent work in the study of β-emission has taken full advantage of these developments, and a number of analyses of the focusing properties of various fields that are suitable for β-spectrometers have been published (1).

Thin-windowed geiger counters are generally used as detectors. Somewhat different conditions from those obtaining in the β-spectrometer prevail in the photoelectric case. The electron energies are much lower, and the electron multiplier (2), operated in the spectrometer vacuum, is now a convenient detector.

Energy losses suffered by the escaping electrons because of collisions within the material can be reduced by using a low-incidence photon beam for producing the photoelectrons near the surface and by studying the electrons that are emitted in a direction near the normal.

2. The 3π/2 Spectrometer

A particularly convenient instrument for these photoelectric studies can be designed by employing a radially varying focusing field and a 3π/2 final-deflection angle. The

electron beam is limited by a narrow slit at the $\pi/2$ position. The geometry of this spectrometer is shown in Fig. IV-1. In contrast with a uniform-field instrument, perfect radial focusing can be obtained for all monoenergetic electrons emitted in the normal direction from the median line of the entire extended specimen. The narrow first slit should ensure a low background level arising from scattered electrons. The field strengths required are not sufficiently high to interfere with the electrostatic focusing of the multiplier, which is placed behind the second slit. Dependence of emission on crystallographic direction in a single-crystal specimen can be conveniently studied with such an arrangement.

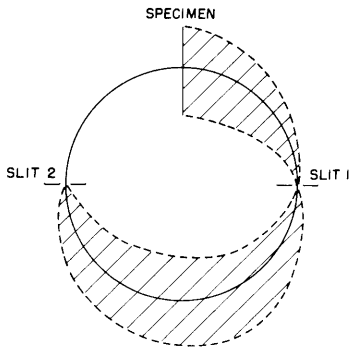

Fig. IV-1. Geometry of the spectrometer.

The variation, in the median plane of the instrument, of the magnetic field required to produce such perfect radial focusing, can be calculated to any desired degree of accuracy by standard perturbation techniques. Several authors have made such a calculation for the 180° analyzer and since, by symmetry, the solutions require that the orbits cross the midplane at right angles, the results of these calculations may be used here. The most reliable work on this problem seems to be that of Beiduk and Konopinski (3) who have performed the calculation to the fifth differential coefficient in the Taylor expansion of the field about the unperturbed orbit and have checked their results by graphical plotting of the orbits obtained. Their result for the field is

$$H(r) = H_o \left\{ 1 - \frac{3}{4}\left(\frac{r - r_o}{r_o}\right)^2 + \frac{7}{8}\left(\frac{r - r_o}{r_o}\right)^3 - \frac{9}{16}\left(\frac{r - r_o}{r_o}\right)^4 + \frac{51}{320}\left(\frac{r - r_o}{r_o}\right)^5 \right\} \qquad (1)$$

where r_o is the radius of the unperturbed orbit.

3. Calculation of Focusing Properties

To construct and operate the $3\pi/2$ spectrometer, it is necessary to calculate the second-order focusing properties, both on and off the median plane, in order to determine the detailed geometrical requirements, such as slit sizes, for a given degree of resolution. In previous analyses of defocusing effects a beam of electrons of fixed velocity has been considered, and the beam "spread" caused by emission from points off the normal orbit and at small angles to the initial direction of this orbit has been calculated. The results are of interest for studying β-emission lines of given energies. For photoelectric emission, however, the analysis must take into account variations in

the emission velocity, in addition to the effects that have been mentioned, since velocity focusing is now of as much interest as directional focusing. The β-spectrometer has, as it were, built-in velocity focusing, in the fixed-energy lines of the spectrum itself.

It is required, therefore, to solve the equations of motion of an electron in the prescribed field through second order in the small deviations from the cylindrical coordinates of the normal orbit and from the desired emission velocity. Cylindrical polar axes are taken with the origin at the center of the spectrometer, z-axis perpendicular to the median plane, and $\theta = 0$ through the specimen surface. The field vector $\vec{H}$ is defined for perfect focusing in the median plane, and its variation as a function of z can be obtained, since the field is solenoidal. Hence

$$\nabla \times \vec{B} = 0 \tag{2}$$

and the continuity equation applies, and so

$$\nabla \cdot \vec{B} = 0 \tag{3}$$

The r and z equations of motion may be written

$$\ddot{r} - r\dot{\theta}^2 = \frac{e}{m} r \dot{\theta} B_z \tag{4}$$

$$\ddot{z} = -\frac{e}{m} r \dot{\theta} B_r \tag{5}$$

and an integral of the motion must be

$$\dot{r}^2 + r^2 \dot{\theta}^2 + \dot{z}^2 = v^2 \tag{6}$$

If we use Eqs. 1-6, and write

$$r = r_o + \rho_1 + \rho_2 \tag{7}$$

$$\dot{\theta} = \omega_o + \omega_1 + \omega_2 \tag{8}$$

$$z = \zeta_1 + \zeta_2 \tag{9}$$

$$v = v_o + v_1 + v_2 \tag{10}$$

the orbits can be solved by perturbation calculations through second order in the small quantities. The details of the calculation will not be carried through here. The results are presented in terms of the following quantities:

α = the deviation of the angle of emission in the median plane from the normal to the surface of the specimen.

β = the deviation of the angle of emission from the normal to the surface of the specimen in the plane containing the normal and the z-axis.

$\epsilon = (r - r_o)/r_o$, the reduced rectangular coordinate of the emission point on the

surface of the specimen in the radial direction of the spectrometer.

η = the reduced rectangular coordinate of the emission point on the surface of the specimen in the z-direction.

$\delta = v_1/v_o$.

The coordinates of the electron position at $\theta = \pi/2$ and $3\pi/2$ with respect to the slit centers can be written as $(\epsilon_{\pi/2}, \eta_{\pi/2})$ and $(\epsilon_{3\pi/2}, \eta_{3\pi/2})$ and are calculated to be

$$\epsilon_{\pi/2} = \alpha + \delta - \frac{3}{4}\eta^2 + \frac{1}{2}\alpha\epsilon + \frac{3}{2}\left(1 - \frac{\pi}{2}\right)\beta\eta + \left(\frac{1}{4} - \pi\right)\epsilon\delta \tag{11}$$

$$\eta_{\pi/2} = \eta + \frac{\pi}{2}\beta + \frac{3}{2}\left(1 - \frac{\pi}{2}\right)\alpha\eta + \left(\frac{3\pi}{4} - 2\right)\epsilon\beta + \frac{3}{2}\left(1 - \frac{\pi}{8}\right)\eta\delta - \frac{3}{2}\epsilon\eta \tag{12}$$

and

$$\epsilon_{3\pi/2} = -\alpha + \delta - \frac{3}{4}\eta^2 - \frac{1}{2}\alpha\epsilon - \frac{3}{2}\left(1 + \frac{3\pi}{2}\right)\beta\eta + \left(3\pi - \frac{9}{4}\right)\epsilon\delta \tag{13}$$

$$\eta_{3\pi/2} = \eta + \frac{3\pi}{2}\beta - \frac{3}{2}\left(1 + \frac{3\pi}{2}\right)\alpha\eta + \left(2 + \frac{9\pi}{4}\right)\epsilon\beta + \frac{3}{2}\left(1 - \frac{27}{16}\pi^2\right)\eta\delta - \frac{3}{2}\epsilon\eta \tag{14}$$

In these expressions only second-order quantities involving ϵ or η are included because these are the terms that are sufficiently large to be of interest.

The terms that do not involve δ agree with those derived by Beiduk and Konopinski (3) when they are calculated for the 180° instrument.

4. Geometrical Aberrations

In order to visualize the defocusing effects resulting from geometrical aberrations of the system let us consider what happens to electrons emitted from a given point of the

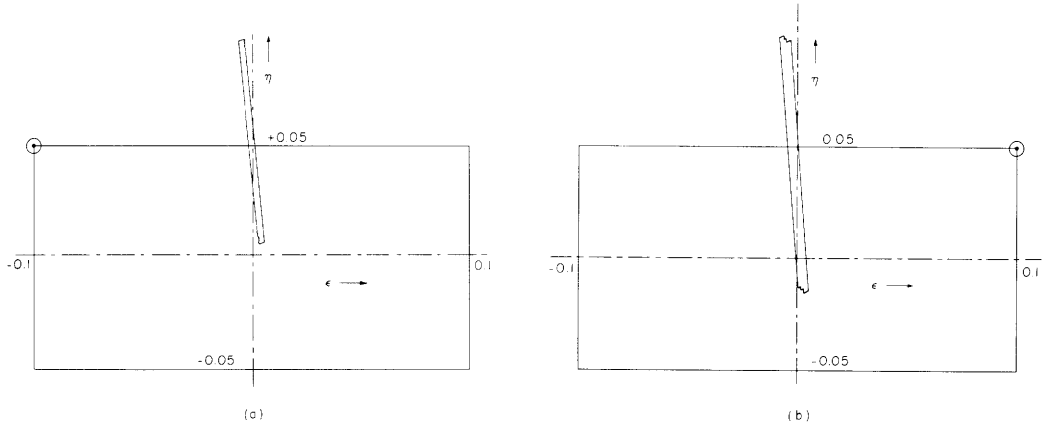

Fig. IV-2. Beam cross sections at $\theta = 3\pi/2$ for emitting points: (a) $\epsilon = -0.1$, $\eta = +0.5$; (b) $\epsilon = +0.1$, $\eta = +0.5$.

specimen within given angular ranges $-\alpha$ to $+\alpha$ and $-\beta$ to $+\beta$. The cross section of such a beam at $\theta = \pi/2$ or $3\pi/2$ can be mapped back onto the specimen surface by an appropriate rotation about the z-axis. Two such diagrams are given in Fig. IV-2, with the beam cross sections at $\theta = 3\pi/2$ for emitting points at extreme positions on the specimen. For a spectrometer of 10-cm radius the specimen represented would have the dimensions 2 cm × 1 cm. The ranges of angles of emission are $-10^{-3} < \alpha < +10^{-3}$ radians and $-10^{-2} < \beta < +10^{-2}$ radians. It is seen that maximum intensity can be obtained by employing curved slits, concave toward the center of the instrument. The equation of the center line for both slits must have the form

$$\epsilon = -\frac{3}{4}\eta^2 \tag{15}$$

5. Velocity Focusing

The slit widths govern the extreme deviations as follows. Let the slits be of equal width, say 2w. From the first-order terms of Eqs. 11 and 13, we have

$$-w < \alpha + \delta < +w \tag{16}$$

and

$$-w < -\alpha + \delta < +w \tag{17}$$

Adding them gives

$$-2w < 2\delta < +2w \tag{18}$$

that is,

$$|\delta| < w \tag{19}$$

Reversing Eq. 17 gives

$$-w < \alpha - \delta < +w \tag{20}$$

and adding this to Eq. 16 gives

$$-2w < 2\alpha < +2w \tag{21}$$

that is,

$$|\alpha| < w \tag{22}$$

If the specimen is assumed to emit electrons, normally to its surface, at equal intensity over a continuous range of velocities, the intensity received through the two slits can be plotted as a function of velocity from Eqs. 11 and 13. We have

$$\epsilon_{\pi/2} = \delta + \left(\frac{1}{4} - \pi\right)\epsilon\delta \tag{23}$$

and

$$\epsilon_{3\pi/2} = \delta + \left(3\pi - \frac{9}{4}\right)\epsilon\delta \tag{24}$$

Electrons for which $\delta = 0$ will be collected from all portions of the specimen, but for $\delta = \delta_{max}$, only those emitted at $\epsilon = 0$ will pass through. For $\epsilon > 0$, electrons will be collected when

$$0 < \epsilon < \frac{\delta_m - \delta}{2.89\,\delta} \tag{25}$$

and for $\epsilon < 0$, when

$$-\frac{\delta_m - \delta}{7.17\,\delta} < \epsilon < 0 \tag{26}$$

where δ_m is written for the maximum value of δ accepted from an emitting point at $\epsilon = 0$, $\eta = 0$. Let $\delta/\delta_m = \Delta$. When $\Delta = 1$, no intensity will be observed; as Δ decreases toward zero, the intensity will be proportional to the range of ϵ from which contributions are possible, and hence

$$I(\delta) \propto \frac{1 - \Delta}{7.17\,\Delta} + \frac{1 - \Delta}{2.89\,\Delta} \tag{27}$$

The intensity will follow Eq. 27 until the quantity $(1 - \Delta)/(2.89\,\Delta)$ reaches the maximum value of ϵ. After this, the contribution of the outer portion of the specimen will remain constant, and the intensity will be given by

$$I(\delta) \propto \left(\frac{1 - \Delta}{7.17\,\Delta} + \epsilon_{max}\right) \tag{28}$$

This will be the case until $(1 - \Delta)/(7.17\,\Delta)$ reaches the magnitude of ϵ_{min}, and after this the intensity will remain constant.

For the case given in Figs. IV-2 and IV-3, in which $|\epsilon_{max}| = |\epsilon_{min}| = 0.1$, we have the following values:

(i) When $1 > \Delta > 0.77$, $I(\delta) = 0.49\left(\frac{1 - \Delta}{\Delta}\right) I_o$ (29)

(ii) When $0.77 > \Delta > 0.58$, $I(\delta) = \left\{0.14\left(\frac{1 - \Delta}{\Delta}\right) + 0.1\right\} I_o$ (30)

(iii) When $0.58 > \Delta > 0$, $I(\delta) = 0.2\, I_o$ (31)

where I_o is a constant of proportionality. A graph of the intensity received as a function of velocity is shown in Fig. IV-3a. If the specimen is moved in its own plane along the radial direction of the spectrometer, so that the ratio of $|\epsilon_{max}|$ to $|\epsilon_{min}|$ is $(3\pi - 9/4)$ to $(\pi - 1/4)$, the discontinuity in the intensity curve of Fig. IV-3a no longer occurs; the distribution for this case is given in Fig. IV-3b.

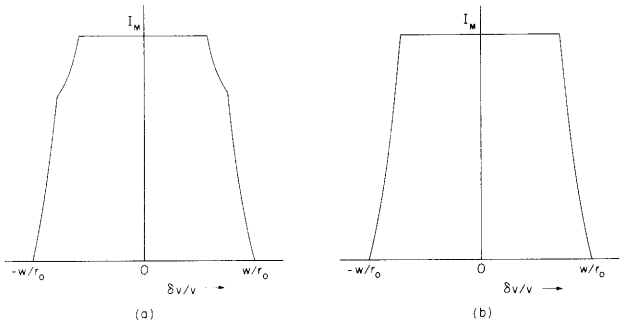

Fig. IV-3. Velocity focusing of the spectrometer; w = slit width, r_o = neutral-orbit radius: (a) symmetrically placed specimen; (b) asymmetrically placed specimen.

If a similar curve is made for the uniform-field spectrometer, the intensity I_o under the conditions stated above is found to be lower by a factor of approximately 20.

A spectrometer with the focusing properties described in this report is proposed for use in studying photoelectric emission in the soft X-ray region. It is hoped that it may also be possible to obtain useful information about the incident radiation itself by studying its photoelectric effect. This program will involve generating the X-rays in both a solid target and in a molecular beam.

E. R. Pike

References

1. See, for instance, G. E. Lee-Whiting and E. A. Taylor, Can. J. Phys. 35, 1 (1957).
2. J. S. Allen, Phys. Rev. 55, 966 (1939).
3. F. M. Beiduk and E. J. Konopinski, Rev. Sci. Instr. 19, 594 (1948).

B. DESIGN OF AN IRON-FREE MAGNET FOR A FOCUSING SPECTROMETER

The field required for the spectrometer described in Section IV-A is radially symmetric and has the following form, as calculated by Beiduk and Konopinski (1).

$$H(r) = H_o \sum_{n=0}^{5} h_n \left[(r - r_o)/r_o\right]^n \qquad (1)$$

where $h_o = 1$, $h_1 = 0$, $h_2 = -3/4$, $h_3 = 7/8$, $h_4 = -9/16$, $h_5 = 51/320$, and r_o is the radius of the unperturbed orbit, which occurs at the maximum value of the field.

The field in the median plane of a pair of Helmholtz coils has radial symmetry, and such a pair may be used as a starting point from which to build up the required field.

Let a be the radius of the coils. Then if s is the distance from the center of one

of the coils to a point on the median plane, and the cosine of the angle between this line and the axis of symmetry is μ, it is calculated that H will be given by

$$H(\mu) = \frac{i}{a} \sum_{n=1}^{\infty} (-1)^{n+1} \frac{1 \cdot 3 \cdot 5 \ldots (2n-1)}{2 \cdot 4 \cdot 6 \ldots 2n} (2\mu)^{2n+1} \, 2n \, P_{2n}(\mu) \tag{2}$$

when $0 < \mu < 0.5$, and by

$$H(\mu) = \frac{i}{a} \left\{ 1 + \sum_{n=1}^{\infty} (-1)^{n} \frac{1 \cdot 3 \cdot 5 \ldots (2n-1)}{2 \cdot 4 \cdot 6 \ldots 2n} \frac{1}{(2\mu)^{2n}} (2n+1) \, P_{2n}(\mu) \right\} \tag{3}$$

when $0.5 < \mu < 1.0$. The $P_{2n}(\mu)$ are Legendre polynomials of order 2n. Computation of the field results in the graph of Fig. IV-4.

A second Helmholtz pair with twice the current and double the radius of the first pair, and wound in the opposite sense, may be added, and the combined field calculated. This field can be expressed as a function of radial distance, r, in the median plane. Then

$$H(r) = H_2(\mu) - H_1(\mu) \tag{4}$$

which, in terms of r, is

$$H(r) = H_2[1/(1 + r^2)^{1/2}] - H_1[1/(1 + 4r^2)^{1/2}] \tag{5}$$

Computation of H(r) for such a combination, with its inner coil of radius j, results in the graph of Fig. IV-5, in which the abscissas, x, are equal to r/j. This field can be expanded in a Taylor series about its maximum x_o, as follows.

$$H_j(r) = \frac{i}{j} \left\{ A_o + A_1 \left(\frac{x - x_o}{x_o} \right) + A_2 \left(\frac{x - x_o}{x_o} \right)^2 + \ldots \right\} \tag{6}$$

or

$$H_j(r) = \frac{i_j}{j} \left\{ A_o + A_1 \left(\frac{r - jx_o}{jx_o} \right) + A_2 \left(\frac{r - jx_o}{jx_o} \right)^2 + \ldots \right\} \tag{7}$$

Equation 7 can be rewritten in the form

$$H_j(r) = \frac{i_j}{j} \left\{ A_o + A_1 \left[\frac{(r - r_o) - (jx_o - r_o)}{jx_o} \right] + A_2 \left[\frac{(r - r_o) - (jx_o - r_o)}{jx_o} \right]^2 + \ldots \right\} \tag{8}$$

where r_o is an arbitrary fixed radius. The terms can be regrouped to give

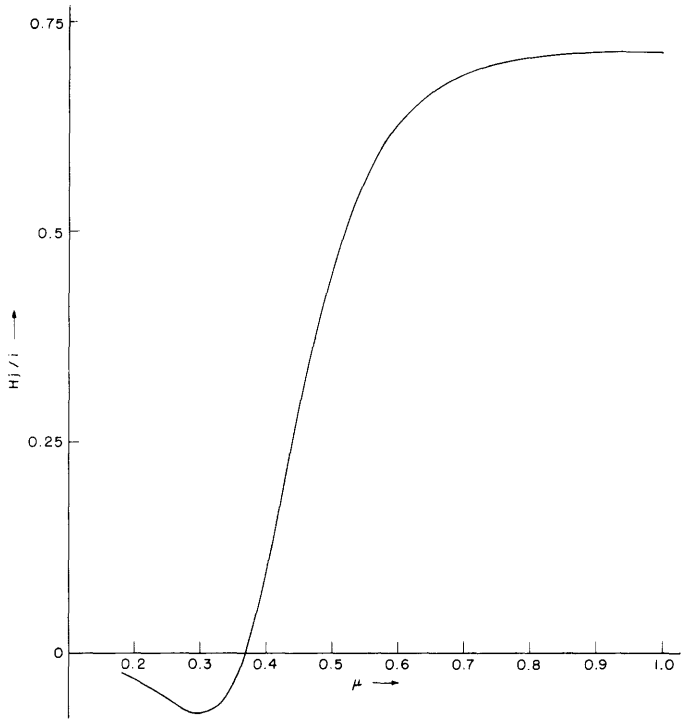

Fig. IV-4. Field in the median plane of a pair of Helmholtz coils.

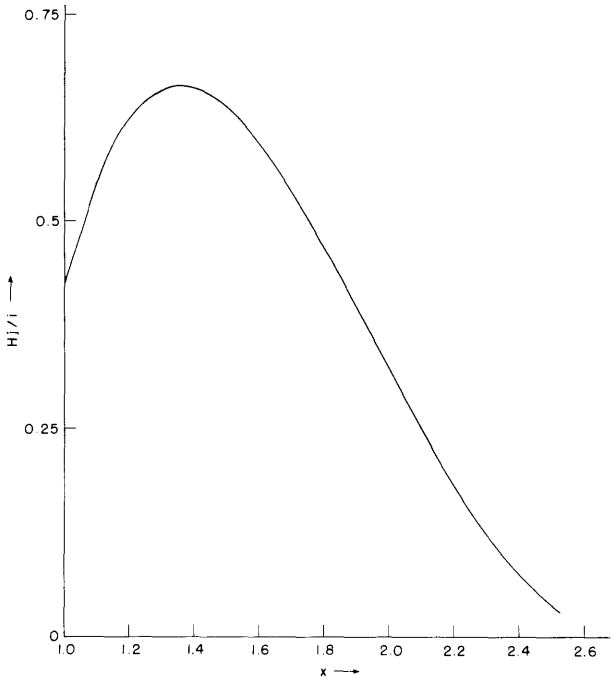

Fig. IV-5. Field of the double-pair combination.

$$H_j(r) = i_j\left\{B_{oj} + B_{1j}\left(\frac{r - r_o}{r_o}\right) + B_{2j}\left(\frac{r - r_o}{r_o}\right)^2 + \ldots\right\} \tag{9}$$

where

$$B_{nj} = \frac{r_o^n}{j^{n+1}\, x_o^n}\left\{A_n - (n+1)\, A_{n+1}\left(\frac{jx_o - r_o}{jx_o}\right) + \frac{(n+1)(n+2)}{1 \cdot 2}\, A_{n+2}\left(\frac{jx_o - r_o}{jx_o}\right)^2 + \ldots\right.$$

$$\left. + (-1)^k\, \frac{(n+1)(n+2)\ldots(n+k)}{1 \cdot 2 \ldots k}\, A_{n+k}\left(\frac{jx_o - r_o}{jx_o}\right)^k + \ldots\right\} \tag{10}$$

Let us consider a continuous winding of coils, as described above, on a former that has the shape of a double cone. If the inner radii range from j_1 to j_2, the resultant field will be

$$H(r) = \int_{j_1}^{j_2} H_j(r)\, dj \tag{11}$$

$$= \int_{j_1}^{j_2} i(j)\, f(r, j)\, dj \tag{12}$$

where

$$f(r, j) = B_{oj} + B_{1j}\left(\frac{r - r_o}{r_o}\right) + B_{2j}\left(\frac{r - r_o}{r_o}\right)^2 + \ldots \tag{13}$$

and $i(j)$ is now to be interpreted as the current density at position j. The current density can be expanded in a Taylor series about the value of jx_o that occurs at r_o, which is chosen to be the radius of the neutral orbit.

$$i(j) = i_o + i_1\left(\frac{jx_o - r_o}{r_o}\right) + i_2\left(\frac{jx_o - r_o}{r_o}\right)^2 + \ldots \tag{14}$$

Thus

$$H(r) = \int_{j_1}^{j_2} \left\{\sum_{m=0}^{\infty} i_m\left(\frac{jx_o - r_o}{r_o}\right)^m\right\}\left\{\sum_{q=0}^{\infty} B_{qj}\left(\frac{r - r_o}{r_o}\right)^q\right\} dj \tag{15}$$

We compare this with the expansion given by Eq. 1 and deduce that

$$H_o\, h_n = \int_{j_1}^{j_2} B_{nj} \sum_{m=0}^{\infty} i_m\left(\frac{jx_o - r_o}{r_o}\right)^m dj \tag{16}$$

The integral can be evaluated by expanding binomially and integrating term by term. Only the result will be given here:

$$H_o\, h_n = \sum_{m=0}^{\infty} \sum_{k=0}^{\infty} \sum_{r=0}^{m+k} i_m (-1)^{k+r} \left(\frac{x_o}{r_o}\right)^{m-n-r} P(n,k)\, Q(m,k,r)\, R(m,n,r)\, A_{n+k} \tag{17}$$

where

$$P(n,k) = \frac{(n+1)(n+2)\ldots(n+k)}{1 \cdot 2 \ldots k} \qquad k \neq 0$$
$$P(n,k) = 1 \qquad k = 0 \tag{18}$$

$$Q(m,k,r) = \frac{(m+k)(m+k-1)\ldots(m+k-r+1)}{1 \cdot 2 \ldots r} \qquad r \neq 0$$
$$Q(m,k,r) = 1 \qquad r = 0 \tag{19}$$

$$R(m,n,r) = \frac{(j_2)^{m-n-r} - (j_1)^{m-n-r}}{m-n-r} \qquad m-n-r \neq 0$$
$$R(m,n,r) = \log_e (j_2/j_1) \qquad m-n-r \neq 0 \tag{20}$$

The values of A_n were found up to A_7 by setting up and solving the required number of simultaneous equations of the form of Eq. 5, and using calculated values from Eq. 4. The curve of Fig. IV-5 was replotted by using the series expansion and found to agree closely with the direct plot.

Equation 17, with the auxiliary Eqs. 18, 19, and 20, allow an air-core magnet to be designed for any desired focusing field. The coefficients, h_n, of the desired field are inserted, which gives a set of simultaneous equations for as many coefficients i_m as are required. The final expression for i(j) may be interpreted as the winding density (ampere turns per centimeter) of a continuously wound coil that has a nonuniform winding.

A number of solutions is possible for any given field. By varying either the value of x_o/r_o, that is, the position of the neutral orbit with respect to the coil, or j_1 and j_2, that is, altering the length of the coil, the graph of winding density as a function of position can be adjusted to give reasonable values for the construction of the coil.

Solutions are being investigated for the spectrometer field specified by the h_n of Eq. 1. We intend to construct a magnet based on these calculations.

E. R. Pike

References

1. F. M. Beiduk and E. J. Konopinski, Rev. Sci. Instr. 19, 594 (1948).

C. CYCLOTRON RESONANCE IN GERMANIUM AT LOW TEMPERATURES

The equation for n-type germanium in an rf electric field and dc magnetic fields that are perpendicular can be written with the inclusion of a tensor collision frequency $\overleftrightarrow{\nu}$ and the effective mass tensor $\overleftrightarrow{m}$.

$$\overleftrightarrow{m} \cdot \overleftrightarrow{\nu} \cdot \vec{v} + e\vec{v} \times \vec{H} + e\vec{E} = \frac{d}{dt}(\overleftrightarrow{m} \cdot \vec{v}) \tag{1}$$

When $\vec{E} = \vec{E}_o e^{i\omega t}$ and $\vec{v} = \vec{v}_o e^{i\omega t}$, Eq. 1 becomes

$$\overleftrightarrow{m} \cdot \overleftrightarrow{\nu} \cdot \vec{v}_o + e\vec{v} \times \vec{H} + e\vec{E}_o = i\omega \overleftrightarrow{m} \cdot \vec{v}_o \tag{2}$$

When the coordinate system is so chosen that Z is in the 111 axis, the y-axis is in the plane of the $\vec{H}$ vector and the 111 direction solution is simplified.

Fairly good generality is obtained by choosing $\vec{E}$ to be perpendicular to H and keeping $\vec{E}$ in the plane formed by the $\vec{H}$ vector and the 111 direction. The $\vec{H}$ vector makes an angle θ with the 111 direction. The solution of Eq. 2 for the microwave power absorbed is

$$\vec{J} \cdot \vec{E} = \frac{\dfrac{ne^2E^2}{m_t \omega_{bt}}(\nu_t - i\omega)\left[\dfrac{\sin^2\theta}{\omega_{bt}}(i\omega - \nu_t) + \dfrac{\cos^2\theta}{\omega_{b\ell}}(i\omega - \nu_\ell)\right]}{\left[(\nu_t - i\omega)(i\omega - \nu_t)(i\omega - \nu_\ell)\dfrac{1}{\omega_{bt}\omega_{b\ell}} - \sin^2\theta(i\omega - \nu_t) - \dfrac{\omega_{bt}}{\omega_{b\ell}}\cos^2\theta(i\omega - \nu_\ell)\right]} \tag{3}$$

where

$$\omega_{bt} = \frac{e}{m_t} H \quad \text{and} \quad \omega_{b\ell} = \frac{e}{m_\ell} H$$

$$\overleftrightarrow{\nu} = \begin{vmatrix} \nu_t & 0 & 0 \\ 0 & \nu_t & 0 \\ 0 & 0 & \nu_\ell \end{vmatrix} \qquad \overleftrightarrow{m} = \begin{vmatrix} m_t & 0 & 0 \\ 0 & m_t & 0 \\ 0 & 0 & m_\ell \end{vmatrix}$$

When $\overleftrightarrow{\nu}$ is isotropic, Eq. 3 reduces to a simpler form. When $\omega \gg \nu_t$ and $\omega \gg \nu_\ell$, this equation will show a large maximum for the absorption at a microwave frequency given by

$$\omega = \left(\sin^2\theta\ \omega_{bt}\omega_{b\ell} + \cos^2\ \omega_{bt}^2\right)^{1/2}$$

which is a standard result.

Determination of an effective collision time, measured from the width of the

microwave absorption versus frequency, has been carried out. Using the condition

$$\left| \frac{(\vec{J} \cdot \vec{E})_{\omega = \omega_b}}{(\vec{J} \cdot \vec{E})_{\omega = \omega_b + \Delta}} \right| = 2$$

an effective collision frequency has been derived

$$\Delta = \sqrt{3}\ \nu_t - \frac{\sqrt{3}}{2} \sin^2\theta (\nu_t - \nu_\ell) \frac{\omega_{bt}\omega_{b\ell}}{\omega_b^2}$$

Experimental (4) and theoretical (5) evidence has been obtained to show that this case applies for ionized impurity scattering in n-type germanium at liquid-helium temperature.

T. Higier

References

1. L. Gold, Anisotropy of hot-electron problem in semi-conductors with spheroidal energy surfaces, Phys. Rev. 104, 1580-1584 (1956).

2. W. Schockley, Cyclotron resonances, magnetoresistance and Brillouin zones in semi-conductors, Phys. Rev. 90, 491 (1953).

3. S. Buchsbaum, An electron in crossed magnetic fields, M.I.T., Sept. 1958 (unpublished).

4. R. A. Laff and H. Y. Fan, Magneto resistance in n-type germanium at low temperatures, Phys. Rev. 112, 317 (1958).

5. F. S. Ham, Ionized impurity scattering in semi-conductors, Phys. Rev. 100, 1251(A) (1955).

D. MEASUREMENT OF RESONANT-FREQUENCY SHIFTS OF A MICROWAVE CAVITY CAUSED BY THE HALL EFFECT IN SEMICONDUCTOR MATERIALS

A theory and a technique for the measurement of plasma densities by utilizing the amount of detuning of a resonant microwave cavity caused by the introduction of the plasma into the cavity have been developed (1). We decided to extend this work, both theoretical and experimental, to the study of the conductivity tensor of semiconductors. It is hoped that from this work techniques for the measurement of semiconductor properties at low temperatures, which could eliminate contact difficulties that might arise, will evolve.

The pertinent theory has been modified to include the presence of a magnetic field directed axially along cylindrical samples that are placed at the center of a microwave cavity operating in the TE_{011} mode at 3 cm. With this configuration the magnetic field is everywhere perpendicular to the probing azimuthal electric field, and thus a

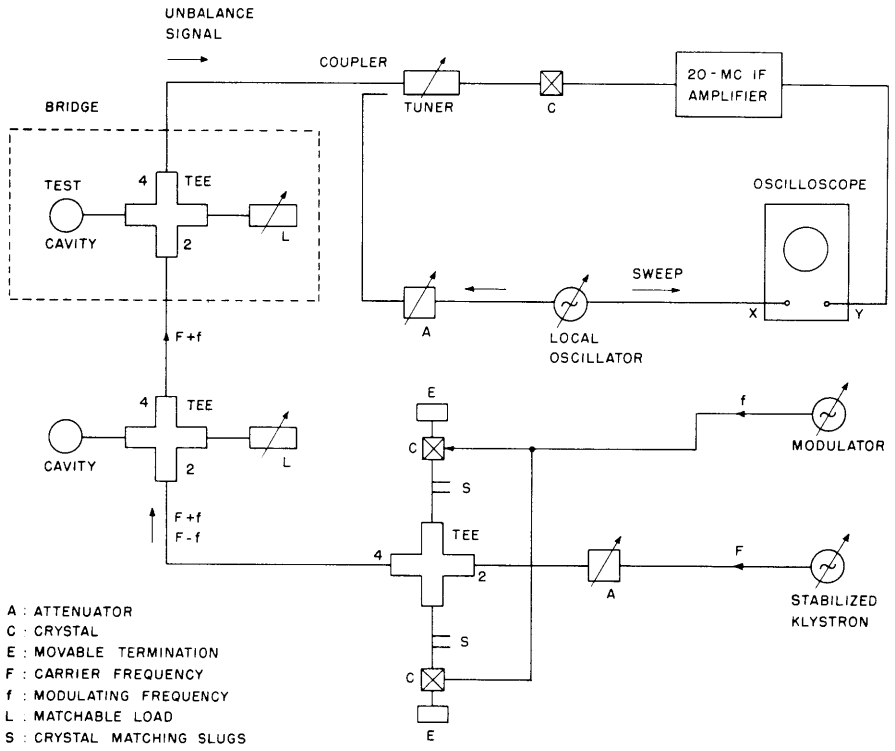

Fig. IV-6. Frequency-shift measurement circuit.

Hall-effect situation that alters the resonant frequency of the cavity because of the generation of a radial component of electric field in the cavity is brought about.

Calculations have indicated that if the experimental check of the extended theory is to be electronically possible, the apparatus must be capable of measuring frequency shifts of less than 10 kilocycles for a loaded-cavity Q of 10,000, at X-band. This requirement takes into account the significant reduction in Q which occurs with the insertion of a semiconductor sample into the cavity.

Referring to Fig. IV-6, a stabilized signal of frequency F is mixed with a modulating signal of frequency f in the conventional manner, by using a magic Tee. By careful adjustment, the carrier frequency is eliminated at the mixer. In order to eliminate subsequent overloading of the amplifiers by an unused signal, one of the two main sidebands, say F - f, is balanced out by another Tee configuration. The remaining strong sideband, F + f, is the test signal. When F + f is at the resonant frequency of the test cavity with the bridge Tee balanced so that there is no output signal, the bridge circuit is at its sharpest possible null position. For a slight unbalance caused by detuning of the test cavity, however, there does exist a nonzero output signal from the bridge. This signal is fed into a modified i-f amplifier of a spectrum analyzer, passes through a high-gain amplifier, and is fed to the Y-input of a saw-tooth-swept oscilloscope for display.

The dispersion of the i-f amplifier has been adjusted so that, for $f \approx 0.7$ mc, higher sidebands than the first do not enter the amplifier chain. This allows full utilization of the available gain and accounts for the good sensitivity of this system.

To obtain the frequency shift that has caused the slight unbalance, f is adjusted to rebalance the bridge. The change in f, read from the modulator dial, is the frequency shift. For small shifts, this is the only adjustment required for making a given measurement, once the system has been initially balanced at the resonant frequency of the test cavity.

Several tests of this system have been carried out on a limited scale. They indicate that this arrangement will fulfill all requirements. First, using a test cavity with a Q of 10,000, and eliminating the major temperature effects on the cavities involved, we observed that the greatest drift over several two-hour periods was approximately 3 kc, in one direction from balance. With the same test cavity, the minimum measurable shift for instantaneous readings was slightly less than 1.0 kc. This procedure is the one that resembles most closely the anticipated experimental procedure. Finally, the original test cavity was replaced by one with an unloaded Q of 3000. There were provisions for sliding a brass slug along the axis of the cavity in order to detune it. This procedure simulated what is to be the ultimate experimental arrangement. As the slug was introduced into the cavity, the smallest frequency shift that could be measured with an accuracy of approximately 10 per cent was ±3 kc.

It may be noted here that the use of sidebands for measuring frequency shifts is by no means a new idea, but the use of a magic Tee in this particular bridge application results in a sensitivity that far exceeds that of any known method of equal simplicity.

R. Weber

References

1. S. J. Buchsbaum and S. C. Brown, Microwave measurements of high electron densities, Phys. Rev. 106, 196-199 (1957).

E. RECOMBINATION OF ELECTRONS WITH DONORS IN GERMANIUM

In Quarterly Progress Report No. 51, page 32, we outlined our results for the measurement of majority carrier recombination in germanium. The theory and the method for measuring the decay of the electron density and the density of compensating impurities were also outlined. Similar measurements have been made over a small range of temperature and the results are shown in Fig. IV-7. It is interesting that the few points that were measured fall on a straight line on a log-log graph, and the temperature dependence of the recombination probability is found to be $T^{-1.8}$, and that of the cross section to be $T^{-2.3}$ (Fig. IV-8).

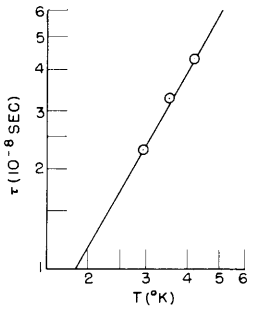

Fig. IV-7. Measured time constants for recombination.

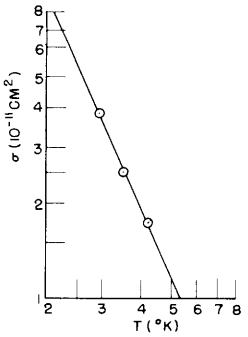

Fig. IV-8. Cross sections calculated from the time constants.

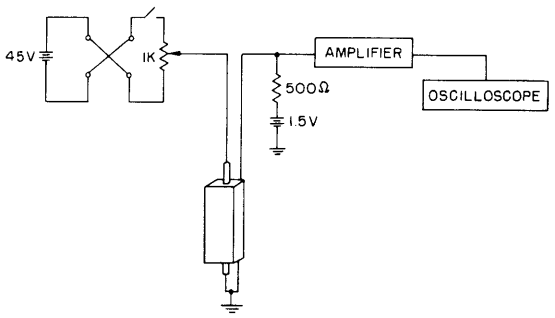

Fig. IV-9. Light detection scheme.

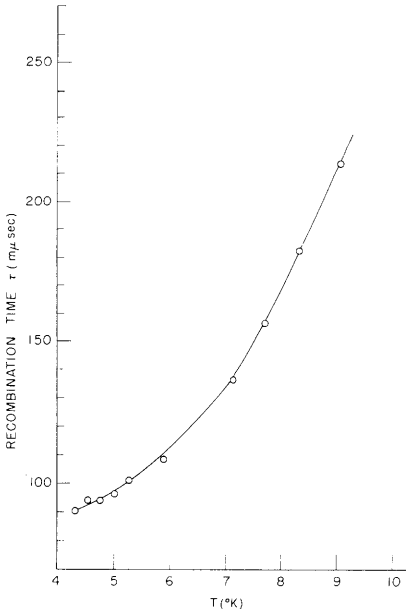

Fig. IV-10. Koenig's results.

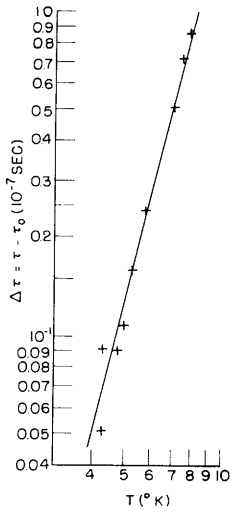

Fig. IV-11. $\Delta\tau$ calculated from Koenig's results.

Theoretical calculations of the recombination cross section, with the assumption of a coincident mechanism in which a phonon and a photon are emitted, predict a temperature dependence of $T^{-2.5}$.

We succeeded in detecting the emission of light during recombination by using a light detector that consists of a germanium parallelepiped along whose axis a hole was bored. The piece of germanium was placed in the hole of the detector so that any light emitted would be absorbed by the parallelepiped (Fig. IV-9), and thus produce a change in conductivity. The germanium used in the detector was a piece of material doped with 10^{16} antimony donors/cc, while the other piece had only 3.8×10^{13} antimony donors/cc (sample BTL-1). The apparatus was housed in a lightproof case and kept in a liquid-helium bath. When sample BTL-1 was almost breaking down, and intermittent increases of current were observed, a large increase of noise appeared on the screen of the oscilloscope. When the field across sample BTL-1 was increased beyond the breakdown voltage, there was a decrease of noise on the oscilloscope screen. The explanation of this behavior is that when the sample is broken down and ampere currents pass through it, there is Joule heating of the sample and a corresponding decrease of the cross section for recombination. The noise seen on the oscilloscope may be attributed to recombination light. It should be noted that such light could have been detected even if its energy was slightly smaller than the binding energy of antimony in the BTL-1 sample. This is so because of the onset of impurity band conductivity in the detector, which results in a decrease of its activation energy.

Some points concerning the recombination scheme are still obscure. Initially, we must account for the discrepancy between the results obtained by Koenig (1) and by the author. Koenig's results are shown in Fig. IV-10. It is seen that at low temperature the measured time constants tend to approach a saturation value, which agrees numerically with what would be expected for a thermal decay in which the phonon mean-free path is limited by sample size. For this case, $\tau = (3\Lambda^2)/(v\lambda)$, where Λ is the diffusion length, λ is the phonon mean-free path, and v is the phonon velocity (2).

If we plot the logarithm of the difference between the measured time constant and the value for saturation as a function of temperature, the resulting points fall on a straight line whose slope is 4 (Fig. IV-11). Such a result is to be expected if Koenig's results represent the decay of an increase of temperature produced by the Joule effect during breakdown, and if the thermal conductivity is limited by Rayleigh scattering of phonons by impurities (2) and by sample size.

The explanation given by Lax (3) for Koenig's result is completely different from ours. Lax developed a theory for recombination in which an electron in the conduction band falls into an excited bound state of an impurity with the emission of a phonon. This electron has, however, a non-negligible probability of being re-excited into the conduction band by absorbing a phonon. The capture mechanism is brought about by successive

falls into more strongly bound states. The last jump, from the first excited state to the ground state of the impurity, can eventually take place with the emission of light. The temperature dependence of such a cross section would be $\sigma \propto T^{-4}$. To explain the saturation effect noticed by Koenig, Lax makes the reader note that if the radii of the excited orbits in which the electrons are captured are comparable with the distances between the impurities, the electrons should be shared between them. This should happen when

$$kT \approx \frac{e^2}{Kd} = \frac{e^2}{K} \sqrt[3]{N_A}$$

where K is the dielectric constant, and d is the distance between impurities. The value of N_A that is necessary for the calculation of the cross section is thus effectively changed and the temperature dependence of the cross section can vary from T^{-4} to T^{0}.

It is clear that the temperature dependence of the cross section cannot by itself determine the recombination mechanism, especially if the range of temperatures over which the recombination is measured is small. Lax's theory foresees a cross section that is independent of the kind of donor impurity, while the phonon-photon theory foresees a strong dependence on the binding energy of the impurities (nearly E^7). This effect is now being investigated by studying the recombination of electrons with arsenic donors.

1. Thermal Effects

If the overvoltage applied to the sample during breakdown is sufficiently large, a time constant other than that arising from recombination appears (Fig. IV-12). This longer "tail" can be moved parallel to itself by changing the applied overvoltage. The time constant does not depend on temperature over the small range studied but on sample size. The theory for thermal decay predicts a time constant $\tau = (3\Lambda^2)/(\lambda v)$, where the factor 3 has its origin in the assumption of an isotropic phonon distribution. When the sample size limits thermal conductivity, the time constant should vary proportionally with the sample size. This is, indeed, the case, so that when the sample cross section was changed from 2×2 mm^2 to 1×1 mm^2 the time constant was halved. The observed time constant is, however, three times longer than that which was calculated from the decay of an isotropic distribution. If we assume that what we see is the decay of the electron density produced by nonequilibrium phonons excited during breakdown, these phonons should have a strongly anisotropic distribution and the direction of propagation parallel to the drift velocity of the electrons should be strongly favored. Since the phonons are mainly traveling along the axis of the sample, it is natural that they should live much longer than when they travel perpendicular to it.

To give further evidence that this phonon beam is produced during breakdown, an experimental arrangement different from that described in previous quarterly progress

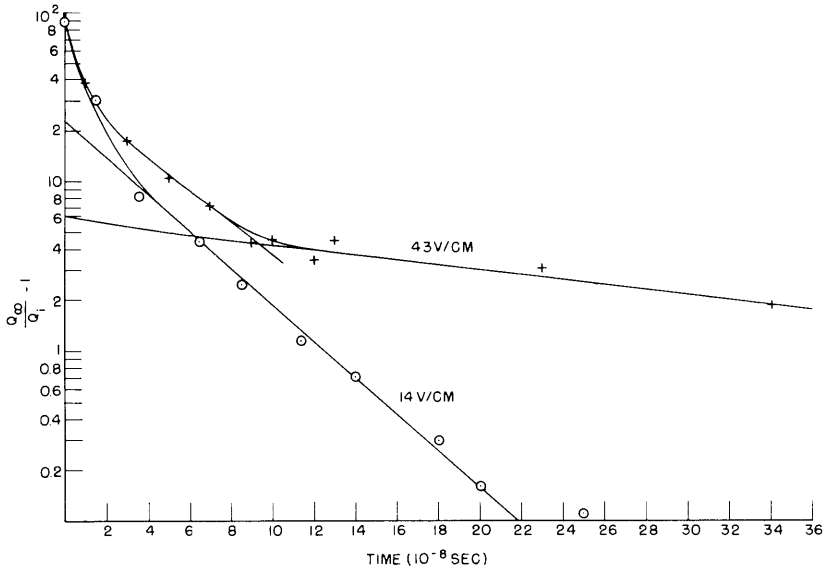

Fig. IV-12. Effect of a large breakdown field.

reports was used. This experiment was suggested by Professor Aigrain (4).

The sample is now mounted partly inside the central part of a re-entrant cavity (Fig. IV-13), and the region in the neighborhood of B is covered with tin, in order to ensure a field-free region inside the semiconductor. The cavity was mounted on one of the symmetric arms of a magic Tee, and on the other there was a matched load. By varying a double-stub tuner on the cavity arm, we could have no microwave power coming out of the E-arm. The experiment consisted in breaking down the region AB of the semiconductor by a dc pulse and trying to detect any change in the region BC of the semiconductor that is in the cavity. Should we have a beam of phonons produced during breakdown, the signal out of the E-arm of the magic Tee would differ according as the drift velocity of the electrons is in or out of the cavity. The results are shown in Fig. IV-14 and confirm this hypothesis. The order of magnitude of the decay time agrees with that of Fig. IV-12, and the delay between the breakdown of section AB and the signal from BC is

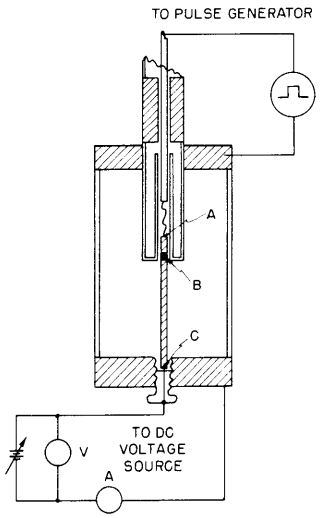

Fig. IV-13. Experimental arrangement for displaying the phonon "beam."

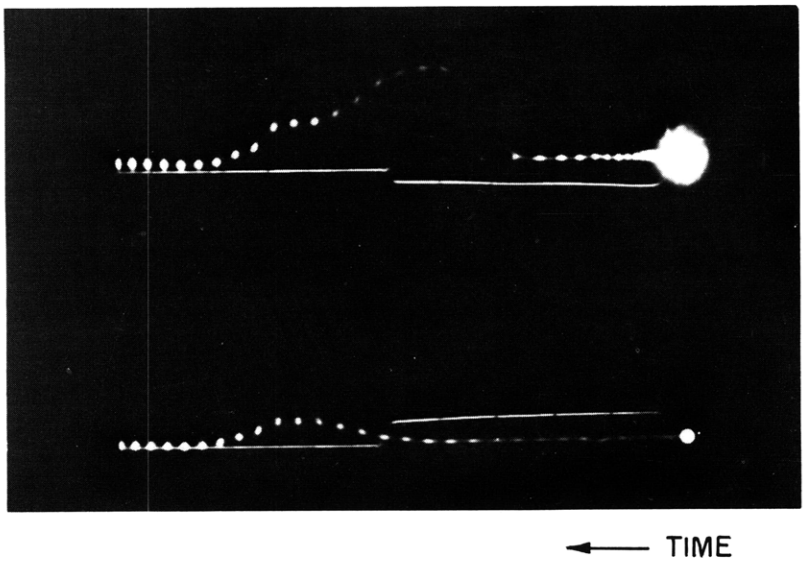

Fig. IV-14. Power output from the E-arm of the magic Tee when a negative (upper trace) or positive (lower trace) pulse is applied to AB. The dots are due to a 10-mc sine wave applied to the z-axis of the oscilloscope.

consistent with what would be expected from phonon propagation. Applying a variable dc field across BC does not affect the phenomenon, as long as the value of the applied field is below the breakdown value. The result is independent of the field applied to BC. Further measurements for determing the collimation of the phonon "beam" are being made.

2. A Fast Microwave Bridge

In relation to the measurements that have just been described, it is of interest to be able to determine the number of phonons progressing in one direction as compared with those going in the opposite direction. The output of the microwave power from the magic Tee does not vary linearly with the changes in standing-wave ratio produced in one of the symmetric arms. Consequently, from the pulses shown in Fig. IV-14, not much can be said quantitatively about this effect. To rebalance the bridge when transient imbalances are produced in the cavity in one of the symmetric arms, a microwave mixer and stub tuner are substituted for the matched load on the other arm. We apply current to the crystal in the mixer so that its impedance is changed sufficiently to produce no output from the E-arm. This is a very sensitive method for measuring small changes in standing-wave ratio and determining their relative time dependence.

G. Ascarelli

[See following page for references.]

References

1. S. H. Koenig, International Conference on Semiconductors, University of Rochester, Rochester, New York, Aug. 18-22, 1958.

2. P. O. Klemens, Proc. Roy. Soc. (London) A208, 108 (1951).

3. M. Lax, International Conference on Semiconductors, University of Rochester, Rochester, New York, Aug. 18-22, 1958.

4. P. Aigrain, private communication (Massachusetts Institute of Technology, Sept. 1958).